HOKKAIDO UNIVERSITY

Title	X-ray absorption fine structure studies on nickel phosphide catalysts for the non-oxidative coupling of methane reaction using a theoretical model
Author(s)	Al Rashid, Md Harun; Dipu, Arnoldus Lambertus; Nishikawa, Yuta et al.
Citation	Radiation Physics and Chemistry, 189, 109727 https://doi.org/10.1016/j.radphyschem.2021.109727
Issue Date	2021-12-01
Doc URL	https://hdl.handle.net/2115/90939
Rights	© <2021>. This manuscript version is made available under the CC-BY-NC-ND 4.0 license http://creativecommons.org/licenses/by-nc-nd/4.0/
Rights(URL)	https://creativecommons.org/licenses/by-nc-nd/4.0/
Type	journal article
File Information	FINAL MANUSCRRIPT-HARUN 20210422xTOTAL -Revise1 (2)aallblackforHascu.pdf

Hokkaido University Collection of Scholarly and Academic Papers : HUSCAP

X-ray absorption fine structure studies on nickel phosphide catalysts for the non-oxidative coupling of methane reaction using a theoretical model

Md Harun Al Rashid[a] , Arnoldus Lambertus Dipu[b], Yuta Nishikawa[b], Hitoshi Ogihara[c], Yuta Inami[b], Shoji Iguchi[b], Ichiro Yamanaka[b], Shinchi Nagamatsu[d], Daiki Kido[d], Bing Hu[d], Kiyotaka Asakura[*d]

[a] Graduate School of Engineering, Hokkaido University, Sapporo 060-8628, Hokkaido, Japan
[b] School of Materials and Chemical Technology, Tokyo Institute of Technology, Tokyo 152-8552, Japan
[c] Graduate School of Science and Engineering, Saitama University, Saitama 338-8570, Japan
[d] Institute for Catalysis, Hokkaido University, Hokkaido 001-0021, Japan

[*] Corresponding author: Institute for Catalysis, Hokkaido University, Kita 21, Nishi 10, Kita-ku, Sapporo, Hokkaido, Japan, 001-0021
Email address: askr@cat.hokudai.ac.jp (Kiyotaka Asakura)

Abstract

SiO_2-supported Ni phosphide catalysts are highly active toward the non-oxidative coupling of methane (NOCM) reaction, and their catalytic activity is strongly dependent on their Ni:P ratio. We analyzed Ni phosphide catalysts using X-ray absorption fine structure (XAFS) to elucidate the structure-catalytic activity relationship. Because only Ni_2P was available as a reference material, we calculated the theoretical XAFS based on the reference crystal structures using the FEFF program and compared them with the experimental spectra of Ni phosphide catalysts. We demonstrated that catalysts with Ni to P ratios of 1:1, 2:1, and 3:1 consisted mainly of the Ni_2P, $Ni_{12}P_5$, and Ni_3P, respectively. We found that Ni_2P exhibited the highest activity toward NOCM because of its optimum balance of C–H cleavage activity and coke formation. This analysis demonstrated that the theoretical XAFS simulation could be used to identify the structure of supported catalysts based on the crystal structure of reference compounds.

Keywords: X-ray absorption, FEFF method, Nickel phosphide, Methane conversion

1. Introduction

Transition-metal Ni phosphides have attracted much attention as highly active catalysts for hydrodesulfurization (HDS) (Oyama, 2003; Oyama et al., 2009; Rodriguez et al., 2003), hydrodenitrogenation (HDN) (Oyama, 2003; Oyama et al., 2009), hydrodeoxygenation (HDO) (Cho et al., 2014; Iino et al., 2019; Zhao et al., 2011), hydrogen evolution reaction (HER) (Hu et al., 2020; Liu and Rodriguez, 2005; Moon et al., 2015; Popczun et al., 2013; Vij et al., 2017), dehydrogenation of cyclohexane (Li et al., 2014), the water-gas shift (WGS) reaction (Liu et al., 2009), water splitting (Menezes et al., 2017), and hydrodechlorination (Liu et al., 2008).

Methane (CH_4) is the main ingredient in natural and shale gases. The efficient conversion of CH_4 to higher hydrocarbons (C_2H_4, C_2H_6, and C_6H_6) as feedstock is a desirable catalytic reaction for CH_4 as a petroleum alternative (Kondratenko et al., 2017; Wang et al., 2017). Non-oxidative coupling of methane (NOCM) reactions have attracted intensive interest for converting CH_4 to higher hydrocarbons (Borkó and Guczi, 2006; Soulivong et al., 2008; Xu and Lin, 1999). Yamanaka and coworkers found that SiO_2-supported Ni phosphide binary catalysts with a Ni to P ratio of 1:1 exhibited the highest catalytic performance for NOCM among various Ni*X* (*X* = various elements) compounds (Dipu et al., 2018, 2020, 2021). In a previous study, we investigated the structure of Ni phosphide catalysts by analyzing SiO_2-supported Ni phosphide compound catalysts using X-ray absorption fine structure (XAFS) (Al Rashid et al., 2020).

XAFS is classified into two energy regimes: X-ray absorption near edge structure (XANES) and extended X-ray absorption fine structure (EXAFS). XANES is the structure in the X-ray absorption spectrum near the edge up to 50 eV region. EXAFS refers to the oscillation that appears 50 eV or more above the X-ray absorption edge. EXAFS arises from the interference between outgoing photoelectrons and singly scattered electrons (Iwasawa and Asakura, 2017). EXAFS analysis provides details about the local structure, such as the coordination number and bond length. EXAFS data are usually analyzed by curve fitting (CF) (Teo et al., 2014). Although EXAFS is a well-established technique, it suffers from several drawbacks. First, the signals are damped quickly at 500–1000 eV if the sample is highly disordered or if the surrounding atoms are low-*Z* elements. Second, it can only provide one-dimensional bonding information. Third, the amount of information is limited by Nyquist theory in the CF analysis (Kido et al., 2020; Stern, 1993). Consequently, a straightforward analysis of complex systems is difficult.

Ni phosphides have different phases: Ni_3P, $Ni_{12}P_5$, Ni_2P, Ni_5P_4, NiP, NiP_2, and NiP_3 (Massalski et al., 1990; Ren et al., 2007). These compounds have complicated structures with different Ni and P sites and different Ni–P and Ni–Ni bond lengths, as shown in Figure S1(a). For example, the two different types of Ni sites in Ni_2P have different Ni–P and Ni–Ni bond lengths (Figure S1(b)) (Bando et al., 2012, 2011; Kawai et al., 2003; Wada et al., 2012a, 2012b; Yuan et al., 2015; Contreras-Mora et al., 2018). In our previous two-shell fitting EXAFS analysis of Ni phosphide NOCM catalysts with Ni:P ratios of 1:1, 2:1, and 3:1, we found that the Ni–P and Ni–Ni bond lengths differed depending on the Ni:P ratio (Table S1). The Ni–Ni bond length decreased with increasing Ni:P ratio. Interestingly, we found that Ni phosphide catalysts on SiO_2 with Ni:P = 3:1 had a shorter Ni–Ni bond length ($R_{Ni–Ni}$ = 2.45 Å) than that in Ni foil ($R_{Ni–Ni}$ = 2.48 Å). However, analysis by CF could not easily specify the structures. By comparing the results with those for Ni_2P reference compounds, we deduced that the Ni phosphide with Ni:P = 1:1 had the Ni_2P structure. However, the structure of other Ni phosphide catalysts with Ni:P ratios of 2:1 and 3:1 was difficult to determine because of a lack of appropriate reference compounds.

In the near-edge region, strong and characteristic XANES signals appear. XANES occurs because of multiple scattering or transitions to empty bound states (Ankoudinov, 1996; Gunter et al., 2002). XANES analysis is a powerful technique for investigating the local structure of complex systems because it is more sensitive to three-dimensional structures and electronic states (Koningsberger et al., 1988). Because theoretical calculations using the FEFF program have enabled us to reproduce the X-ray absorption fine structure spectra in both the XANES and EXAFS regions (Bosman and Thieme, 2009; Rehr and Albers, 2000), we attempted to analyze the structure of Ni phosphide catalysts by comparing with the theoretical XANES and EXAFS spectra of reference compounds based on their crystal structures instead of by comparing with their experimental XANES and EXAFS spectra. In the present work, we carried out structural analyses of Ni phosphide catalysts on SiO_2 with initial Ni:P ratios of 1:1, 2:1, and 3:1 using theoretical models without the use of experimental reference compounds.

2. Experimental

SiO_2-supported Ni phosphide catalysts (Ni-P/SiO_2) with different Ni and P ratios of 1:1, 2:1, and 3:1 were prepared from $Ni(NO_3)_2{\cdot}6H_2O$ and $(NH_4)_2HPO_4$ precursors by a conventional impregnation method. The preparation details were available elsewhere (Dipu et al., 2018). The samples are denoted by their initial Ni:P ratio; for example, the notation Ni-P/SiO_2 (Ni:P = 1:1) indicates that the molar ratio of Ni to P was 1:1.

X-ray absorption fine structure (XAFS) spectra were recorded at the BL9C beamline of the Photon Factory (PF: 2.5 GeV, 450 mA) at the Institute for Materials Structure Science (KEK-IMSS-PF). The X-rays were monochromatized by a Si(111) double crystal and were focused by a Rh-coated bent cylindrical mirror. The higher harmonics were rejected by the mirror. The Ni K-edge data were collected in a transmission mode. The incident and transmitted X-rays were detected by 100% N_2 gas-filled and (15% N_2 and 85% Ar) mixed-gas-filled ionization chambers, respectively. The EXAFS analyses were carried out using the REX2000 software (Rigaku Co) (Asakura, 1996). Fourier transformed range was 3-16 $Å^{-1}$ for the experimental and theoretical data analysis.

The theoretical XANES and EXAFS spectra were calculated using the FEFF8 code (Zabinsky et al., 1995), which uses self-consistent multiple scattering with a muffin-tin potential (Rehr and Albers, 2000). For the exchange-correlation potential, the Hedin–Lundqvist complex potential was used to obtain fine spectra with a typical full-potential multiple scattering (FMS) radius of 5.0 Å for theoretical XANES calculations. Interestingly, a smaller FMS radius of 3.0 Å gave broad spectra, whereas the 5.0 Å FMS radius calculation sharpened the peak features (Figure S2). The parameters used for the XANES calculations are listed in Table S2. The goodness of fit was defined as R-factor(R (%)) given by

$$R-factor(\%) = \frac{\Sigma_i \left(\chi_{cal}(k_i)-\chi_{obs}(k_i)\right)^2}{\Sigma_i \left(\chi_{obs}(k_i)\right)^2} \times 100,$$

where $\chi_{obs}(k_i)$and $\chi_{cal}(k_i)$ are the experimental and the calculated EXAFS oscillations, respectively.

3. Results and Discussion

Figure 1 compares Ni K-edge XANES, inversely Fourier Transform (IFT) and Fourier Transform (FT) of the Ni_2P reference sample with the FEFF8-calculated theoretical spectra. The experimental and theoretical XANES spectra of Ni_2P show the same three features (labeled A, B, and C in Figure 1).

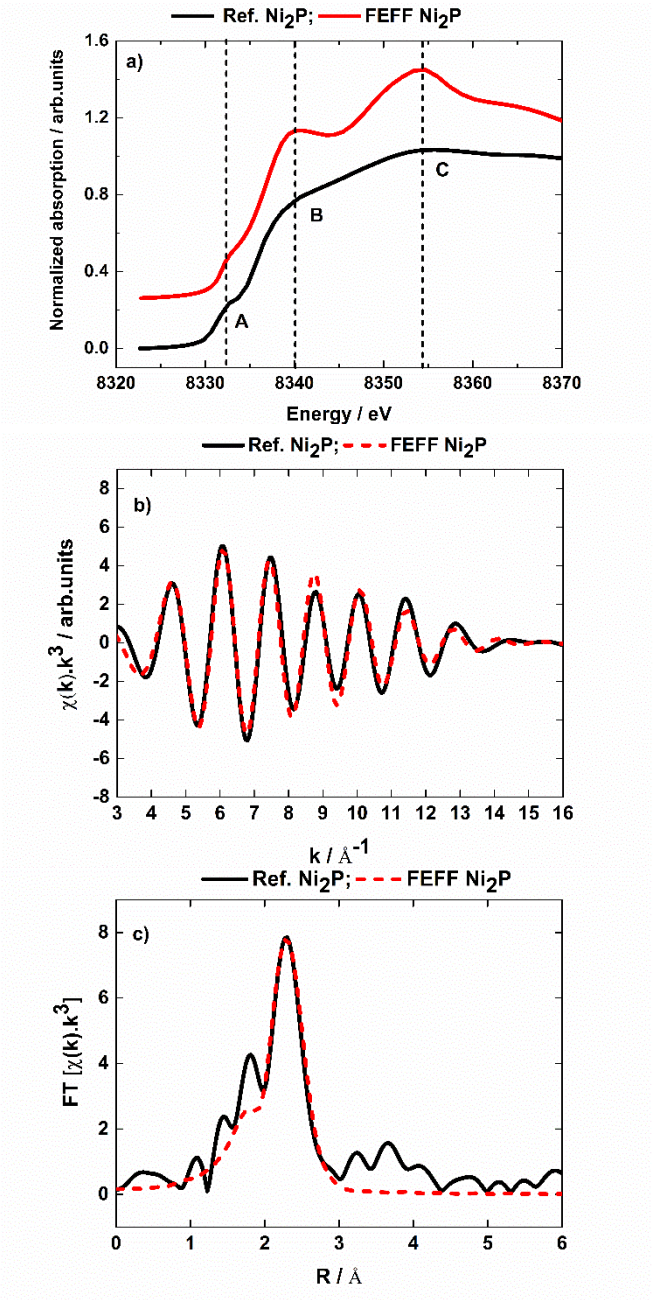

Fig. 1. a) Comparison of experimental and theoretical Ni K-edge XANES spectra of Ni_2P; b) comparison of experimental (solid line) and theoretical Ni K-edge EXAFS (red broken line) spectra of Ni_2P; c) corresponding Fourier transform.

To estimate the systematic error, we compared the peak positions in the experimental and calculated Ni_2P spectra. The differences between the experimental and calculated peak energies were 0.0, −0.4, and 0.0 eV for features A, B, and C, respectively (Table 1).

Table 1
Experimental and theoretical peak positions in XANES of Ni_2P.

	Ref. Ni_2P (eV)	FEFF8 Ni_2P (eV)	ΔE (eV)
A	8332.7	8332.7	0.0
B	8339.7	8340.1	−0.4
C	8354.7	8354.7	0.0

Thus, the experimental and calculated peak positions coincide to each other within ±0.4 eV. Peaks B and C were broadened in the experimental XANES spectrum. Our observation of peak broadening with a smaller FMS radius in the FEFF calculation (Figure S2) suggests that the broadening may arise from the shorter coherence length of photoelectrons in the Ni_2P crystal. Notably, however, the peak position was independent of the FMS radius. Thus, we herein concentrate mainly on the peak positions in the comparison of the experimental and calculated data.

We also used the FEFF8 program to carry out an EXAFS simulation based on the Ni_2P crystal structure. The simulation well reproduced the experimental data for Ni_2P (Figure 1 (b)). This approach differs from the CF method in that the simulated EXAFS spectrum was calculated based on the coordinates of all atoms (Ni and P) without any adjustable parameters except the amplitude reduction factor (S_0^2) and the Debye–Waller factors (σ^2), which had been optimized. By contrast, in the CF analysis, eight parameters were optimized (coordination number (*CN*), bond distance (*R*), Debye–Waller factor (σ^2), and edge-shift (ΔE) for both Ni–Ni, and Ni–P bonds). Although the CF analysis gave much better fitting results (0.5 % in CF vs. 5.8 % in the EXAFS simulation as shown in Table S3), the obtained parameters were not directly related to the real structure, and further interpretation was required. The FEFF simulation approach based on the crystal structure enabled us to elucidate the catalyst structures, although the goodness of fit was worse. We attempted to predict the structures of Ni-P/SiO_2 with different Ni:P ratios in a similar manner.

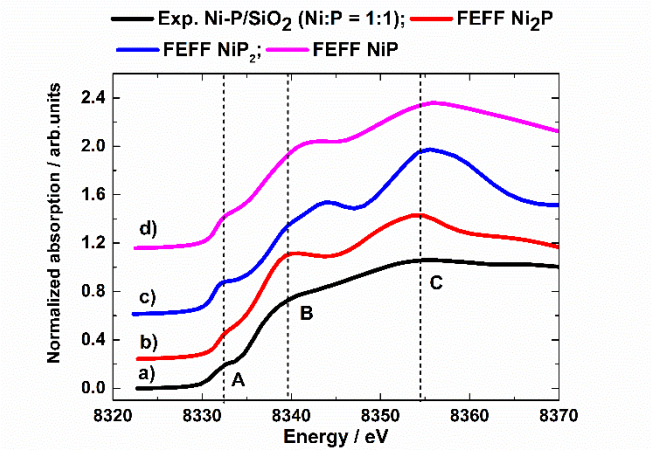

Fig. 2. Comparison of Ni K-edge XANES spectra for a) Ni-P/SiO_2 (Ni:P = 1:1) (black), b) FEFF Ni_2P (red), c) FEFF NiP_2 (blue), and d) FEFF NiP (pink).

Figure S3 shows XANES spectra of Ni-P/SiO_2 with Ni:P ratios of 1:1, 2:1, and 3:1; the spectra show three different peaks (denoted A, B, and C) at different energy positions for Ni-P/SiO_2 (Ni:P = 1:1) and (Ni:P = 3:1). By contrast, the Ni-P/SiO_2 (Ni:P = 2:1) spectrum shows four peaks (A, B, C, and D). Figure S4 shows the FEFF-calculated theoretical XANES spectra of NiP_3, NiP_2, NiP, Ni_5P_4, Ni_2P, $Ni_{12}P_5$, and Ni_3P. Figure S5 shows details of the peak energies for all of the experimental and theoretical Ni K-edge XANES spectra. The calculated XANES spectra for different Ni phosphides show three peaks, whereas the NiP_2 and $Ni_{12}P_5$ spectra show four peaks. We observed a pre-edge peak (denoted as A) in all of the theoretical XANES spectra and assigned this peak to *s*–*d* transitions. Its intensity depends on the degree of *p*–*d* hybridization, which is higher for a tetrahedral structure (Oyama et al., 2009). Figure S6 shows overlapped theoretical XANES spectra in the pre-edge region around peak A. Peak A decreased in intensity with increasing Ni:P ratio. However, a tetrahedral structure was not observed in NiP_3, NiP_2, or NiP. Thus, the pre-edge peak A was not a direct indicator of the presence of a tetrahedral structure in the Ni phosphide compounds.

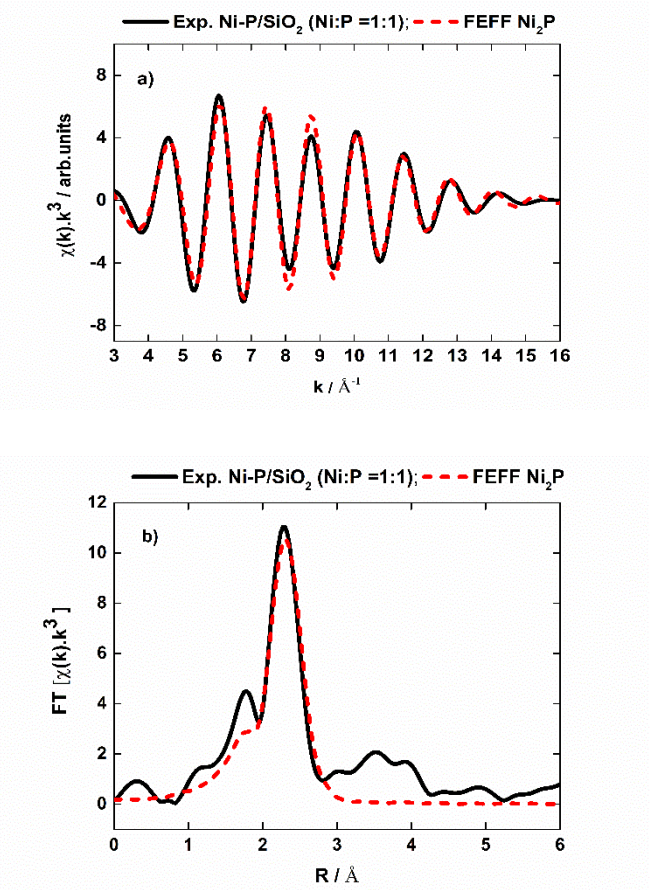

Fig. 3. a) Comparison between theoretical Ni_2P (red broken line) and experimental EXAFS spectra of Ni-P/SiO_2 (Ni:P = 1:1) (black line); (b) corresponding Fourier transform.

Figure 2 shows the Ni K-edge XANES spectrum of Ni-P/SiO_2 (Ni:P = 1:1), together with those of Ni_2P, NiP_2, and NiP calculated using FEFF8. The experimental XANES spectrum of Ni-P/SiO_2 (Ni:P = 1:1) shows three main peaks (A, B, and C). The Ni K-edge peak pattern in the theoretical XANES spectrum of the reference Ni_2P compound agrees with the experimental spectrum of Ni-P/SiO_2 (Ni:P = 1:1). Peaks A, B, and C in its theoretical XANES spectrum appeared at positions corresponding to Ni-P/SiO_2 (Ni:P =

1:1): 8332.7, 8339.7, and 8354.7 eV (Table S4). The theoretical XANES spectra of the other reference compounds show peaks at different positions, as summarized in Table S4. These results suggest that Ni-P/SiO_2 (Ni:P = 1:1) had predominantly the Ni_2P structure. These results agree with our previous results, where we analyzed EXAFS spectra using a conventional CF method (Al Rashid et al., 2020). In this previous studies, two waves corresponding to Ni–Ni and Ni–P bond lengths were observed (Table S1), although Ni_2P had a more complex structure with two different Ni sites, resulting in two different Ni–P and two Ni–Ni bond lengths for each site (Figure S1(b)). As previously mentioned, the Ni–P and Ni–Ni bond lengths obtained by the CF analysis did not directly correspond to the actual structure. In many cases, it was impossible to perform a CF analysis for all bonds because of the Nyquist limitation of the number of fitting parameters (Stern, 1993).

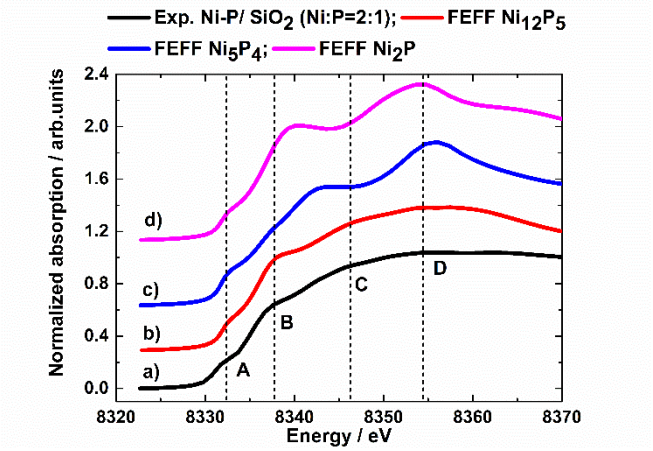

Fig. 4. Comparison of Ni K-edge XANES spectra: a) Ni-P/SiO_2 (Ni:P = 2:1) (black line), b) FEFF $Ni_{12}P_5$ (red line), c) FEFF Ni_5P_4 (blue line), and d) FEFF Ni_2P (pink line).

Here, we calculated the EXAFS oscillation based on the Ni_2P crystal structure and compared the spectrum with that of the Ni-P/SiO_2 (Ni:P = 1:1) catalyst in *k*- and *R*-spaces, as shown in Figures 3 (a) and (b). We found good agreement between the experimental and calculated spectra. The R-factor was 4.0 %. In this analysis, we used an S_0^2 of 0.9 and σ^2 values of 0.009 and 0.0095 Å^2 for Ni–P and Ni–Ni bonds, respectively. By theoretical approaches, we concluded that the Ni-P/SiO_2 (Ni:P = 1:1) consisted mainly of the Ni_2P structure, consistent with a previous report (Al Rashid et al., 2020). We applied the same methods to the other Ni phosphide catalysts.

Figure 4 shows a comparison of the experimental and theoretical XANES spectra of Ni-P/SiO_2 (Ni:P = 2:1). Four peaks (A, B, C, and D) appear in the spectra. The experimental spectrum agrees well with the theoretical Ni K-edge XANES spectrum of $Ni_{12}P_5$ (see also Table S5). For this composition, the energy differences between the experimental and theoretical peak positions are all within ±0.4 eV. The theoretical XANES spectra for other compositions show larger deviations in peak positions from the experimental spectrum. Consequently, we concluded that the experimental spectrum was consistent with the phase $Ni_{12}P_5$.

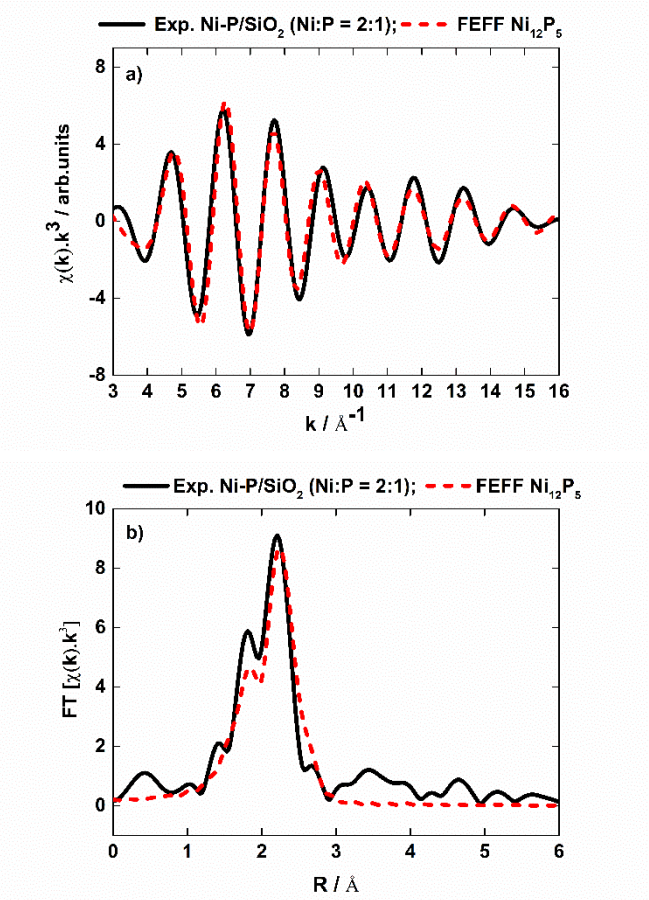

Fig. 5. a) Comparison between theoretical $Ni_{12}P_5$ (red broken line) and experimental Ni-P/SiO_2 (Ni:P = 2:1) (black line) EXAFS spectra, and b) corresponding Fourier transform.

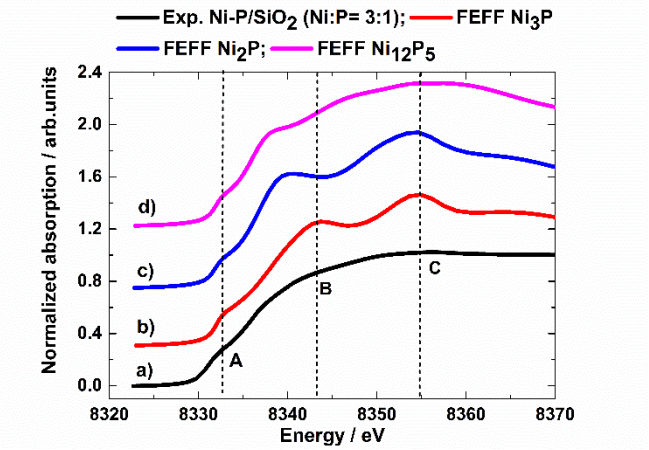

Fig. 6. Comparison of Ni K-edge XANES spectra: a) Ni-P/SiO_2 (Ni:P = 3:1) (black line), b) Ni_3P FEFF (red line), c) Ni_2P FEFF (blue line), and d) $Ni_{12}P_5$ FEFF (pink line).

We then calculated the EXAFS spectrum based on the $Ni_{12}P_5$ crystal structure. Figure 5 (a) compares the experimental EXAFS spectrum of Ni-P/SiO_2 (Ni:P = 2:1) with the theoretical spectrum of $Ni_{12}P_5$, along with the corresponding FTs. The Fourier peak positions correspond well with each other (Figure 5(b)). The S_0^2

factors for Ni–P and Ni–Ni were both fixed at 0.9, and the σ^2 factors were fixed at 0.007 and 0.0075 Å^2, respectively. The R-factor was 10.0%.

Figure 6 shows a comparison of the experimental XANES spectrum of Ni-P/SiO_2 (Ni:P = 3:1) and the calculated spectra of three Ni-rich reference compounds. The XANES structure was immensely broad in the experimental data. We checked the second derivatives to confirm the presence of three peaks (Figure S7). Consequently, we observed three peaks (A, B, and C) in the spectrum of Ni-P/SiO_2 (Ni:P = 3:1). The peak positions corresponded well with the peak positions in the theoretical Ni_3P spectrum (Figure 6 and Table S6).

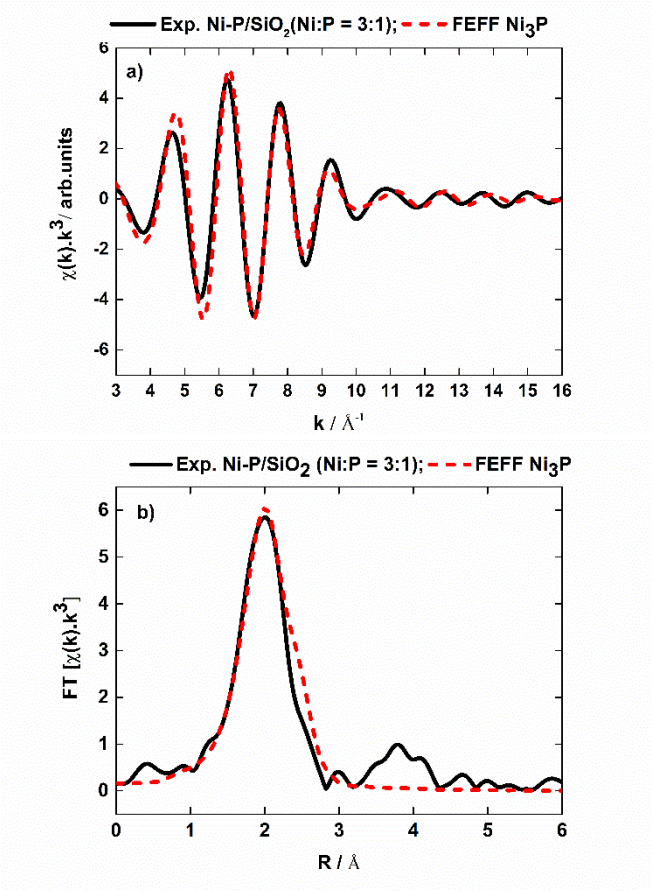

Fig. 7. a) Comparison between theoretical Ni_3P (red broken line) and experimental (black line) EXAFS spectra of Ni-P/SiO_2 (Ni:P = 3:1) (black line); b) corresponding Fourier transforms.

We simulated theoretical EXAFS spectra based on the Ni_3P crystal structure. The S_0^2 and σ^2 values for Ni–P and Ni–Ni were set at 0.9 and 0.009 Å^2, respectively. Figure 7 shows the theoretical EXAFS spectra for the Ni_3P structure, the experimental EXAFS spectra for Ni-P/SiO_2 (Ni:P = 3:1), and their corresponding FTs. We found that the calculated EXAFS data successfully reproduced the experimental data. The R-factor was 7.2 %. In particular, we observed a single peak in the FT of the Ni-P/SiO_2 (Ni:P = 3:1) spectrum and the Ni_3P spectrum (Figure 7 (b)). Thus, we confirmed the formation of the Ni_3P phase in Ni-P/SiO_2 catalysts with an initial Ni:P ratio of 3:1.

The structures of Ni-P/SiO_2 with Ni:P ratios of 1:1, 2:1, and 3:1 were identified as Ni_2P, $Ni_{12}P_5$, and Ni_3P, respectively, based on the theoretical FEFF calculations of their XANES and EXAFS spectra. In the case of Ni-P/SiO_2 samples with Ni:P = 1:1 and Ni:P = 2:1, the Ni:P ratio in the precursor was greater than the Ni:P ratios in the resultant Ni_2P and $Ni_{12}P_5$ because, during the preparation processes under reductive conditions at high temperature, P was volatilized as PH_3. Additional P atoms were, therefore, necessary and were supplied by the reduction of coexisting PO_4 (Bando et al., 2011). Ni_2P lost more P than $Ni_{12}P_5$, and $Ni_{12}P_5$ lost substantially more P than Ni_3P. The presence of more Ni might have prevented the loss of P from the sample due to the Ni adsorption ability which decreases with the increase of P (Kiskinova and Goodman, 1981).

In these analyses, we only used the theoretical reference XANES and EXAFS spectra calculated by FEFF. By comparing the experimental and theoretical XANES data for Ni_2P, we observed that the experimental XANES peaks were broadened and thus we concentrated on the peak position energy. We found that, even if the structures of Ni phosphide compounds were complicated, we could predict an unknown structure by comparing the experimental data with the theoretical XANES and EXAFS data without recording the spectra of the corresponding reference compounds experimentally.

Table 2
Nickel-Nickel bond distances of various nickel phosphide catalysts.

Compound Name	R_{Ni-Ni} (Shortest)^{CF*a} (Å)	R_{Ni-Ni} (Shortest)$^{The.*b}$ (Å)	R_{Ni-Ni} (Average) (Å)
Ni_2P	2.62±0.02	2.61	2.65
$Ni_{12}P_5$	2.52±0.02	2.53	2.58
Ni_3P	2.45±0.02	2.44	2.60

[a] Al Rashid et al., 2020; [b] Ren et al., 2007

In the case of NOCM reactions, Ni-P/SiO_2 (Ni:P = 1:1) exhibited the highest catalytic performance among the investigated Ni phosphide catalysts. The Ni-P/SiO_2 (Ni:P = 1:1) structure corresponded to Ni_2P. More Ni-rich phosphide compounds such as $Ni_{12}P_5$ and Ni_3P exhibited lower activity. Pure metallic Ni efficiently activated the C–H bond in CH_4 and decomposed the CH_4 to coke, which poisoned and deactivated the Ni surface. In the crystal structure of Ni_2P, the shortest Ni–Ni bond length is 2.61 Å (Table 2). In $Ni_{12}P_5$ and Ni_3P, the shortest Ni–Ni bond lengths are 2.53 Å and 2.44 Å, respectively. These shorter bond lengths might have led to the higher activity for C–H bond cleavage in CH_4 and the formation of coke that suppressed the catalytic activity. A higher P content increases the Ni–Ni bond length, which decreases Ni activity. Thus, an appropriate Ni:P ratio provides a good balance between CH_4 activity and preventing coke formation during NOCM reactions. The Ni_2P/SiO_2 catalyst had a suitable Ni:P balance that activated the large amount of methane to the methyl radical than the $Ni_{12}P_5/SiO_2$ and Ni_3P/SiO_2 and consequently form ethane, ethylene, benzene, and so on (Dipu et al., 2018).

Interestingly, a CF analysis of Ni–P compounds with Ni:P = 2:1 and Ni:P = 3:1 gave Ni–Ni bond lengths of 2.52 and 2.45 Å (Table 2), which agreed well with the shortest values for $Ni_{12}P_5$ and Ni_3P. This good correlation is attributed to the fact that the EXAFS CF analysis is more sensitive to the rising part of the radial distribution curve or the shortest bond length (Koningsberger et al.,

1988). When we compared the average Ni–Ni bond length for each crystal structure (Table 2), we could not establish a relationship between bond length and catalytic activity. Further theoretical investigations are necessary to clarify this.

4. Conclusions

In the present work, we analyzed Ni K-edge XANES and EXAFS spectra of Ni phosphide catalysts and determined the crystal structure by comparison with theoretically calculated XANES and EXAFS spectra. The catalytic activity of SiO_2-supported Ni phosphide catalysts in NOCM followed the order Ni_3P < $Ni_{12}P_5$ < Ni_2P. The theoretical XANES and EXAFS simulation approach predicted the local structure of unknown supported metal catalysts with complex structures. This approach may open a new way to reveal the complex structure of heterogeneous catalysts.

Author statement

Any data will be available upon request.

Declaration of competing interest

The authors declare that they have no known competing financial interests or personal relationships that could have appeared to influence the work reported in this paper.

Acknowledgments

We performed these experiments under the CREST project “Innovative Catalysts" JPMJCR15P4 of Japan Science and Technology (JST). All the XAFS work was performed at KEK-PF under proposal numbers 2016G546 and 2018G628. We thank all XAFS team members at the Photon Factory for their technical support.

Appendix. Supporting informtion

Supporting information data for this article can be found online.

References

Al Rashid, M.H., Dipu, A., Nishikawa, Y., Ogihara, H., Inami, Y., Obuchi, S., Yamanaka, I., Nagamatsu, S., Kido, D., Asakura, K., 2020. Active Phase Structure of the SiO2-supported Nickel Phosphide Catalysts for Non-oxidative Coupling of Methane (NOCM) Reactions. e-Journal Surf. Sci. Nanotechnol. 18, 24–27. https://doi.org/10.1380/ejssnt.2020.24

Ankoudinov, A.L., 1996. Relativistic Spin-dependent X-ray Absorption Theory. University of Washington. http://leonardo.phys.washington.edu/PAPERS/dissertations/thesis_ankudinov.pdf

Asakura, K., 1996. Analysis of EXAFS, in: Y. Iwasawa (Ed.), “X-Ray Absorption Fine Structure for Catalysts and Surfaces.” World Scientific, Singapore, pp. 33–58. https://doi.org/10.1142/9789812830838_0003

Bando, K.K., Koike, Y., Kawai, T., Tateno, G., Oyama, S.T., Inada, Y., Nomura, M., Asakura, K., 2011. Quick X-ray absorption fine structure studies on the activation process of Ni2P supported on K-USY. J. Phys. Chem. C 115, 7466–7471. https://doi.org/10.1021/jp111657z

Bando, K.K., Wada, T., Miyamoto, T., Miyazaki, K., Takakusagi, S., Koike, Y., Inada, Y., Nomura, M., Yamaguchi, A., Gott, T., Ted Oyama, S., Asakura, K., 2012. Combined in situ QXAFS and FTIR analysis of a Ni phosphide catalyst under hydrodesulfurization conditions. J. Catal. 286, 165–171. https://doi.org/10.1016/j.jcat.2011.10.025

Borkó, L., Guczi, L., 2006. Non-oxidative methane transformations into higher hydrocarbons over bimetallic Pt-Co catalysts supported on Al2O3 and NaY. Top. Catal. 39, 35–43. https://doi.org/10.1007/s11244-006-0035-4

Bosman, E., Thieme, J., 2009. Modeling of XANES-spectra with the FEFF-program, in: Journal of Physics: Conference Series. https://doi.org/10.1088/1742-6596/186/1/012004

Cho, A., Kim, H., Iino, A., Takagaki, A., Ted Oyama, S., 2014. Kinetic and FTIR studies of 2-methyltetrahydrofuran hydrodeoxygenation on Ni 2 P/SiO 2. J. Catal. 318, 151–161. https://doi.org/10.1016/j.jcat.2014.07.021

Contreras-Mora, J., Ariga-Miwa, H., Takakusagi, S., Williams, C.T., Asakura, K., 2018. Phosphorous Diffusion Through Ni2P - Low Energy Diffusion Path and Its Unique Local Structure. J. Phys. Chem. C 122, 6318–6322. https://doi.org/10.1021/acs.jpcc.7b12367

Dipu, A.L., Obuchi, S., Nishikawa, Y., Ogihara, H., Yamanaka, I., 2018. Nickel phosphide catalyst for direct dehydrogenative conversion of methane to higher hydrocarbons, in: The 8th Tokyo Conference on Advanced Catalytic Science and Technology (TOCAT8). Tokyo, pp. P1235, 2018. https://doi.org/https://www.shokubai.org/tocat8/pdf/Poster/P1235.pdf

Dipu, A.L., Ohbuchi, S., Nishikawa, Y., Iguchi, S., Ogihara, H., Yamanaka, I., 2020. Direct Nonoxidative Conversion of Methane to Higher Hydrocarbons over Silica-Supported Nickel Phosphide Catalyst. ACS Catal. 10, 375–379. https://doi.org/10.1021/acscatal.9b03955

Dipu, A.L., Nishikawa, Y., Inami, Y., Iguchi, S., Yamanaka, I., 2021. Development of Highly Active Silica-Supported Nickel Phosphide Catalysts for Direct Dehydrogenative Conversion of Methane to Higher Hydrocarbons. Catal. Lett. https://doi.org/ 10.1007/s10562-021-03612-w

Gunter, K.K., Miller, L.M., Aschner, M., Eliseev, R., Depuis, D., Gavin, C.E., Gunte, T.E., 2002. XANES spectroscopy: a promising tool for toxicology: a tutorial. Neurotoxicology 23, 127–46. https://doi.org/10.1016/s0161-813x(02)00034-7

Hu, C., Lv, C., Liu, S., Shi, Y., Song, J., Zhang, Z., Cai, J., Watanabe, A., 2020. Nickel phosphide electrocatalysts for hydrogen evolution reaction. Catalysts. https://doi.org/10.3390/catal10020188

Iino, A., Takagaki, A., Kikuchi, R., Oyama, S.T., Bando, K.K., 2019. Combined In Situ XAFS and FTIR Study of the Hydrodeoxygenation Reaction of 2-Methyltetrahydrofuran on Ni 2 P/SiO 2. J. Phys. Chem. C 123, 7633–7643. https://doi.org/10.1021/acs.jpcc.8b03246

Iwasawa, Y., Asakura, K., Tada, M. (Eds.), 2017. XAFS Techniques for Catalysts, Nanomaterials, and Surfaces, XAFS Techniques for Catalysts, Nanomaterials, and Surfaces. Springer International Publishing, Cham. https://doi.org/10.1007/978-3-319-43866-5

Kawai, T., Sato, S., Suzuki, S., Chun, W.J., Asakura, K., Bando, K.K., Matsui, T., Yoshimura, Y., Kubota, T., Okamoto, Y.,

Lee, Y.K., Oyama, S.T., 2003. In Situ X-ray Absorption Fine Structure Studies on the Structure of Nickel Phosphide Catalyst Supported on K-USY. Chem. Lett. 32, 956–957. https://doi.org/10.1246/cl.2003.956

Kido, D., Uemura, Y., Wakisaka, Y., Ariga-Miwa, H., Takakuasgi, S., Asakura, K., 2020. Thorough search analysis of extended X-ray absorption fine structure data for complex molecules and nanomaterials applications. e-Journal Surf. Sci. Nanotechnol. 18, 249–261. https://doi.org/10.1380/EJSSNT.2020.249

Kiskinova, M., Goodman, D.W., 1981. Modification of chemisorption properties by electronegative adatoms: H2 and CO on chlorided, sulfided, and phosphided Ni(100). Surf. Sci. 108, 64–76. https://doi.org/10.1016/0039-6028(81)90358-7

Kondratenko, E. V., Peppel, T., Seeburg, D., Kondratenko, V.A., Kalevaru, N., Martin, A., Wohlrab, S., 2017. Methane conversion into different hydrocarbons or oxygenates: Current status and future perspectives in catalyst development and reactor operation. Catal. Sci. Technol. 7, 366–381. https://doi.org/10.1039/c6cy01879c

Koningsberger, D., Prins, R., 1988. X-ray absorption: Principles, applications, techniques of EXAFS, SEXAFS, and XANES, Wiley, New York. https://lib.ugent.be/catalog/rug01:001696179

Li, J., Chai, Y., Liu, B., Wu, Y., Li, X., Tang, Z., Liu, Y., Liu, C., 2014. The catalytic performance of Ni2P/Al2O3 catalyst in comparison with Ni/Al2O3 catalyst in dehydrogenation of cyclohexane. Appl. Catal. A Gen. 469, 434–441. https://doi.org/10.1016/j.apcata.2013.09.047

Liu, P., Rodriguez, J.A., 2005. Catalysts for Hydrogen Evolution from the [NiFe] Hydrogenase to the Ni 2 P(001) Surface: The Importance of Ensemble Effect. J. Am. Chem. Soc. 127, 14871–14878. https://doi.org/10.1021/ja0540019

Liu, P., Rodriguez, J.A., Takahashi, Y., Nakamura, K., 2009. Water–gas-shift reaction on a Ni2P(001) catalyst: Formation of oxy-phosphides and highly active reaction sites. J. Catal. 262, 294–303. https://doi.org/10.1016/j.jcat.2009.01.006

Liu, X., Chen, J., Zhang, J., 2008. Hydrodechlorination of chlorobenzene over silica-supported nickel phosphide catalysts. Ind. Eng. Chem. Res. 47, 5362–5368. https://doi.org/10.1021/ie7017542

Massalski, T.B., Okamoto, H., International., A.S.M., 1990. Binary Alloy Phase Diagrams, in: Alloy Phase Diagrams. ASM International, Materials Park, Ohio, pp. 89–89. https://doi.org/10.31399/asm.hb.v03.a0006247

Menezes, P.W., Indra, A., Das, C., Walter, C., Göbel, C., Gutkin, V., Schmeißer, D., Driess, M., 2017. Uncovering the Nature of Active Species of Nickel Phosphide Catalysts in High-Performance Electrochemical Overall Water Splitting. ACS Catal. 7, 103–109. https://doi.org/10.1021/acscatal.6b02666

Moon, J.-S., Jang, J.-H., Kim, E.-G., Chung, Y.-H., Yoo, S.J., Lee, Y.-K., 2015. The nature of active sites of Ni 2 P electrocatalyst for hydrogen evolution reaction. J. Catal. 326, 92–99. https://doi.org/10.1016/j.jcat.2015.03.012

Oyama, S.T., 2003. Novel catalysts for advanced hydroprocessing: transition metal phosphides. J. Catal. 216, 343–352. https://doi.org/10.1016/S0021-9517(02)00069-6

Oyama, S.T., Gott, T., Asakura, K., Takakusagi, S., Miyazaki, K., Koike, Y., Bando, K.K., 2009. In situ FTIR and XANES studies of thiophene hydrodesulfurization on Ni 2P/MCM-41. J. Catal. 268, 209–222. https://doi.org/10.1016/j.jcat.2009.09.018

Popczun, E.J., McKone, J.R., Read, C.G., Biacchi, A.J., Wiltrout, A.M., Lewis, N.S., Schaak, R.E., 2013. Nanostructured Nickel Phosphide as an Electrocatalyst for the Hydrogen Evolution Reaction. J. Am. Chem. Soc. 135, 9267–9270. https://doi.org/10.1021/ja403440e

Rehr, J.J., Albers, R.C., 2000. Theoretical approaches to x-ray absorption fine structure. Rev. Mod. Phys. 72, 621–654. https://doi.org/10.1103/RevModPhys.72.621

Ren, J., Wang, J. Guo, LI, J. Fen, LI, Wang, Y. 2007. Density functional theory study on crystal nickel phosphides. Ranliao Huaxue Xuebao/Journal Fuel Chem. Technol. 35, 458–464. https://doi.org/10.1016/S1872-5813(07)60029-2

Rodriguez, J.A., Kim, J.-Y., Hanson, J.C., Sawhill, S.J., Bussell, M.E., 2003. Physical and Chemical Properties of MoP, Ni 2 P, and MoNiP Hydrodesulfurization Catalysts: Time-Resolved X-ray Diffraction, Density Functional, and Hydrodesulfurization Activity Studies. J. Phys. Chem. B 107, 6276–6285. https://doi.org/10.1021/jp022639q

Soulivong, D., Norsic, S., Taoufik, M., Copéret, C., Thivolle-Cazat, J., Chakka, S., Basset, J.M., 2008. Non-oxidative coupling reaction of methane to ethane and hydrogen catalyzed by the silica-supported tantalum hydride: (≡SiO)2Ta-H. J. Am. Chem. Soc. 130, 5044–5045. https://doi.org/10.1021/ja800863x

Stern, E.A., 1993. Number of relevant independent points in x-ray-absorption fine-structure spectra. Phys. Rev. B 48, 9825–9827. https://doi.org/10.1103/PhysRevB.48.9825

Teo B.K., 2017. Chapter 6. Data Analysis. Berlin; Heidelberg, pp. 295–406. https://doi.org/10.1201/9781315158839-7

Vij, V., Sultan, S., Harzandi, A.M., Meena, A., Tiwari, J.N., Lee, W.G., Yoon, T., Kim, K.S., 2017. Nickel-based electrocatalysts for energy-related applications: Oxygen reduction, oxygen evolution, and hydrogen evolution reactions. ACS Catal. 7, 7196–7225. https://doi.org/10.1021/acscatal.7b01800

Wada, T., Bando, K.K., Miyamoto, T., Takakusagi, S., Oyama, S.T., Asakura, K., 2012a. Operando QEXAFS studies of Ni 2P during thiophene hydrodesulfurization: Direct observation of Ni-S bond formation under reaction conditions. J. Synchrotron Radiat. 19, 205–209. https://doi.org/10.1107/S0909049512001197

Wada, T., Bando, K.K., Oyama, S.T., Miyamoto, T., Takakusagi, S., Asakura, K., 2012b. Operando observation of Ni 2P structural changes during catalytic reaction: Effect of H 2S pretreatment. Chem. Lett. 41, 1238–1240. https://doi.org/10.1246/cl.2012.1238

Wang, B., Albarracín-Suazo, S., Pagán-Torres, Y., Nikolla, E., 2017. Advances in methane conversion processes. Catal. Today 285, 147–158. https://doi.org/10.1016/j.cattod.2017.01.023

Xu, Y., Lin, L., 1999. Recent advances in methane dehydro-aromatization over transition metal ion-modified zeolite catalysts under non-oxidative conditions. Appl. Catal. A Gen. 188, 53–67. https://doi.org/10.1016/S0926-860X(99)00210-0

Yuan, Q., Ariga, H., Asakura, K., 2015. An Investigation of Ni2P Single Crystal Surfaces: Structure, Electronic State and Reactivity. Top. Catal. https://doi.org/10.1007/s11244-015-0360-6

Zabinsky, S.I., Rehr, J.J., Ankudinov, A., Albers, R.C., Eller, M.J., 1995. Multiple-scattering calculations of x-ray-absorption

spectra. Phys. Rev. B 52, 2995–3009. https://doi.org/10.1103/PhysRevB.52.2995

Zhao, H.Y., Li, D., Bui, P., Oyama, S.T., 2011. Hydrodeoxygenation of guaiacol as model compound for pyrolysis oil on transition metal phosphide hydroprocessing catalysts. Appl. Catal. A Gen. 391, 305–310. https://doi.org/10.1016/j.apcata.2010.07.039